scientific reports

Check for updates

OPEN

Real-time static unbalance evaluation of the Cardan shaft equipped in high-speed train based on nonzero frequency filter

Hu Yongxu✉, Luo Kang, Yang Yaru & Luo Yan

To reduce the upsprung weight, cardan shafts are equipped in high-speed train to transmit torque from motor to gearbox. The driving safety and stability of the train are closely related to the condition of the cardan shaft, which may experience unbalance during operation. Therefore, vibration sensors are installed on the train to monitor the condition of the cardan shaft. In this study, a mechanical model of the cardan shaft was developed to elucidate the unbalance force characteristics of the cardan shaft with static unbalance. Based on the analysis of the unbalance force, a narrow bandpass filter constructed using the nonzero frequency filter (NZFF) was employed to extract unbalance signals from the measured signals. A double integration in time is applied to the extracted signal to eliminate the effect of circular frequency on the signal amplitude and mitigate signal noises caused by track irregularities. Efficient value of the extracted signal was used as an index to evaluate the static unbalance of the cardan shaft. Effects of mechanical suspension structures on value of the index were considered. Kalman filter was utilized to enhance the stability of the evaluated static unbalances. According to the experimental results, the static unbalances were accurately evaluated by the NZFF method.

Keywords Cardan shaft, Static unbalance evaluation, Nonzero frequency filter, High-speed train, Double integration, Kalman filter

To reduce the upsprung weight, cardan shaft is used in Chinese high-speed train CRH5 and German high-speed train ICE. The cardan shaft transmits torque from motor to gearbox (see Fig. 1), and due to wear of wear pad installed in cardan joint, the cardan shaft may become unbalanced[1]. Inertial force generated by the unbalanced cardan shaft led to gearbox failure and motor bolts fractured[2,3], which does harm to driving safety and riding comfort of the train. Therefore, acceleration sensors were installed on gearbox and motor of the train to monitor condition of the cardan shaft[4].

The prerequisite for monitoring the condition of cardan shaft using vibration signals is a thorough understanding of the transmission characteristics of cardan shaft. To understand transmitting characteristics of cardan joint, F.Schemelz et al.[5] introduced the basic theory of shaft driven by the cardan joint comprehensively. Patel and Darpe[6] investigated the harmonic characteristics of excitations generated by misaligned rotors, and effectively utilized full spectra and orbit plots to reveal the distinct features of misalignment faults. Patel[7,8] analyzed the influence of misalignment on the forcing characteristics of flexible coupling followed by experimental investigations. Verma A K et al.[9] presented an approach to distinguish between vibration and electric current signals of a normally aligned motor and a misaligned motor. Lu et al.[10] analyzed the dynamic response of an universal joint with clearances. Omar et al.[11]. examined the impact of static angular misalignment in universal yokes on the vibration characteristics of cardan shaft transmission systems. Their findings revealed that for static angular misalignments exceeding 20 degrees, the proposed phase angle arrangement could reduce torsional vibrations by over 10% and substantially diminish lateral vibrations. Tchomeni and Alugongo[12] investigated the vibratory responses of a twin-rotor system with a universal joint, considering the effects of crack-induced damage and shaft unbalance. Their findings revealed that the time-varying stiffness caused by the breathing crack is the primary factor contributing to the frequency-modulated characteristics of the interconnected twin-rotor system. Xia et al.[13] conducted a comprehensive numerical and experimental analysis of the coupled torsional-lateral vibrations in a 4WD driveline system. The study revealed that the universal joint introduced an external excitation force in the lateral direction, and torsional-lateral vibrations were initiated when twice the

School of Mechanical Engineering, Chengdu University, Chengdu 610000, China. ✉email: huyongxu@cdu.edu.cn

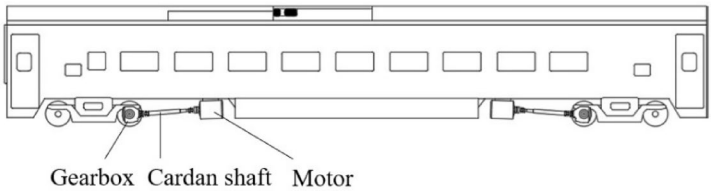

Fig. 1. Diagram of cardan shaft transmission structure.

input rotational speed coincided with either the torsional or lateral natural frequency. SoltanRezaee et al.[14,15] conducted a comprehensive investigation into the oscillatory behavior and resonance phenomenon of a driveline system comprising three elastic shafts interconnected by universal joints. Their findings revealed that variations in the angle of the first U-joint and the characteristics of the intermediate shaft significantly influenced machine instability of the driveline system. Furthermore, they demonstrated that system stability could be enhanced through geometric modifications, increased shaft damping, and adjustments to stiffness. Bharti and Samantaray[16] examined the Sommerfeld effect in a driveline consisting of two cardan joints with large joint angles. Their results indicated that the Sommerfeld effect occurs near half of the critical speed corresponding to the system's torsional vibration natural frequency, as well as near the critical speed itself. Yao and DeSmidt[17] developed a nonlinear rotor-dynamics model for a segmented driveshaft connected by two U-joints, incorporating the effects of angular misalignment and load torque, to investigate the rotor speed capture phenomena induced by driveline misalignment. Their findings demonstrated that the misalignment-induced rotor speed capture could occur when the shaft speed approached half of the first elastic torsional natural frequency, and this phenomenon is influenced by the level of misalignment and motor torque. Since the rotational speed of the cardan shaft in the high-speed train is significantly lower than its critical speed, the unbalance force generated by the cardan shaft under unbalanced conditions constitutes the primary focus of this study's analysis.

Based on signals acquired through the sensors installed in the train equipping the cardan shaft, methods were developed by scholars to assess condition of the cardan shaft. For the condition monitoring of the cardan shaft in high-speed trains, Ding et al.[18] proposed a novel approach to detect the static unbalance of the cardan shaft by employing the double decomposition and double reconstruction method (DDDR). Wavelet and singular value decomposition (SVD) were used to decompose and reconstruct the acceleration signal, and the amplitudes of the Fourier spectrum of the reconstructed signals served as indices for evaluating the unbalance. Although Ding's results demonstrated that the proposed method could effectively extract signal components associated with the cardan shaft static unbalance from the signals collected in bench tests, the proposed method had not been validated on the signals measured through line tests. Zheng et al.[19] proposed a method for extracting feature signals related to cardan shaft static unbalance based on the improved tunable Q-factor wavelet transform (TQWT) method, and established the relationship between the static unbalance and the amplitude intensity (AI) of the Fourier transform of the acceleration signal using a radial basis function neural network. Although a dynamic model was constructed by Zheng to illustrate the relation between the offsets leading to the static unbalance and AI values, spectral leakage of Fourier transform had not been considered by Zheng's study. Ding and Yi[20,21] adopted ensemble empirical mode decomposition (EEMD) to estimate performances of the cardan shaft in real time, however, time costs for calculating intrinsic mode functions (IMFs) had not been optimized in their study. Due to the lack of an efficient algorithm for rapid IMF calculation, the EEMD may not be suitable for real-time estimation of the cardan shaft static unbalance. Li et al.[22] examined the influence of morphological operators and filtering scales on the extraction performance of unbalance signals using morphological filters. They proposed a novel gradient convolution operator and a new fault sensitivity measurement algorithm to develop an enhanced morphological filter for diagnosing static unbalance in cardan shafts. The adaptive notch filter bank is also utilized to extract the unbalance signals of the cardan shaft. Wu et al.[23] employed the filter bank to track the harmonics embedded in the vibrational signal of the cardan shaft and extracted the unbalance signal based on the frequency tracking results of these harmonics. Since cardan shaft is a component of rotating machinery, the methods used for calculating the signal characteristics of rotating machinery can also be applied to assess the condition of the cardan shaft. Blaut and Brenkacz[24] introduced a method for evaluating the operational condition of rotary machines by applying dispersion entropy with a sliding window. They further analyzed the impact of window length on the effectiveness of the proposed method and indicated that a window length of at least two vibration periods of the focused signal is necessary for the method to function properly. Guo et al.[25] developed an adaptive multi-scale improved differential filter to enhance the identification of transient impulses for rotating machine fault diagnosis. Wang et al.[26] designed a specific morphological gradient diagonal slice operator and an enhanced adaptive time-varying morphological filter to accurately diagnose the early faults of rolling bearings.

As acceleration signals generated by the unbalance force due to the static unbalance are periodical and sinusoidal, narrow bandpass filter can be used to extract the unbalance signals. Zero frequency filter (ZFF) was widely used to construct narrow bandpass filters[27,28]. Chauhan and Singh[29] developed a multi-frequency approach for fault identification of bearings and gears using narrowband filters constructed by ZFF. However, the frequency-shifting implemented in their approach reduced its efficiency, thereby increasing the difficulty of real-time analysis of the measured signals. Murty and Yegnanarayana[30] utilized nonzero frequency filter (NZFF) to construct narrowband filter centered around the targeted frequency to extract epoch in voiced speech, and results of the study indicated that the narrowband filter performed prior than the Hilbert envelop

or the group-delayed method. Kumar et al.[31] proposed a method combining minimum entropy deconvolution with convolution adjustment and ZFF, where ZFF was utilized to retain only the localized disturbances at the impulse locations. Sachan et al.[32] proposed a two-level de-noising algorithm for periodic impulses identification, and ZFF was used to enhance the impulse information. The NZFF is a second-order bandpass filter, and the frequency shifting of signal is not required by the NZFF, therefore filtering of signals implemented by the NZFF is relatively efficient.

This study proposes a method to extract unbalanc signals from the measured acceleration signals through NZFF, and utilizes double integral to eliminate the effect of circular frequency on the signal amplitude and mitigate signal noises caused by track irregularities. Based on the amplitude modulation characteristics of cardan shaft vibration induced by the train transmission system's suspension structure, this study subsequently develops a method for evaluating the static unbalance of the cardan shaft using indicators of the extracted signals. Firstly, waveform and frequential feature of the acceleration signal relating to the unbalanced cardan shaft is investigated; then, formulas for calculating parameters of the NZFF to extract the unbalance signals from the measured signals are introduced; next, evaluating methods of the static unbalance of the cardan shaft are demonstrated; finally, the effectiveness of the proposed method is validated by both signals measured from the line tests and collected during train operation.

NZFF construction

A diagram of the cardan joint transmission is given by Fig. 2, the circular frequency of the drive shaft and the driven shaft connected by the cardan joint are denoted as ω_c and ω_c', respectively. The angle between axis of the drive shaft and that of the connecting shaft is denoted by φ.

The relation between ω_c and ω_c' is expressed by Eq. (1), and the formula for calculating the unbalance force generated by the unbalanced cardan shaft during rotation is expressed by Eq. (2).

$$\omega_c' = \frac{\cos\varphi}{1-\sin^2\varphi\sin^2(\omega_c t)} \cdot \omega_c \tag{1}$$

$$F = U\omega_c'^2. \tag{2}$$

where the U is commonly regarded as the static unbalance of the shaft. A frame is defined to demonstrate the projection of the unbalance force onto the signal measurement direction of the sensors installed on the train. The origin of the defined frame is set at the center of the cross shaft connected with the drive shaft, and the x-axis is defined as extending along the direction of the drive shaft, which is also parallel to the longitudinal direction of the train. The z-axis is defined as extending along the vertical direction of the train, and the y-axis is defined as extending along the lateral direction of the train. The point P marked in the figure denotes the center of the cross shaft connected with the driven shaft. The measurement directions of sensors installed on the gearbox and the motor are along the direction of the z-axis, and the formula for calculating the projection of the unbalance force on the z-axis is given by Eq. (3).

$$F_z = F \cdot \cos(\omega_c t) \cdot \sqrt{1-\left(\frac{y_P}{x_P}\cos\omega_c t + \frac{z_P}{x_P}\sin\omega_c t\right)^2}. \tag{3}$$

where the variables x_P, y_P, and z_P denote the x-, y-, and z-coordinates of the point P in the defined reference frame, with units in meters. According to the structure of the train's transmission system, y_P=0 m, x_P=1.73 m,

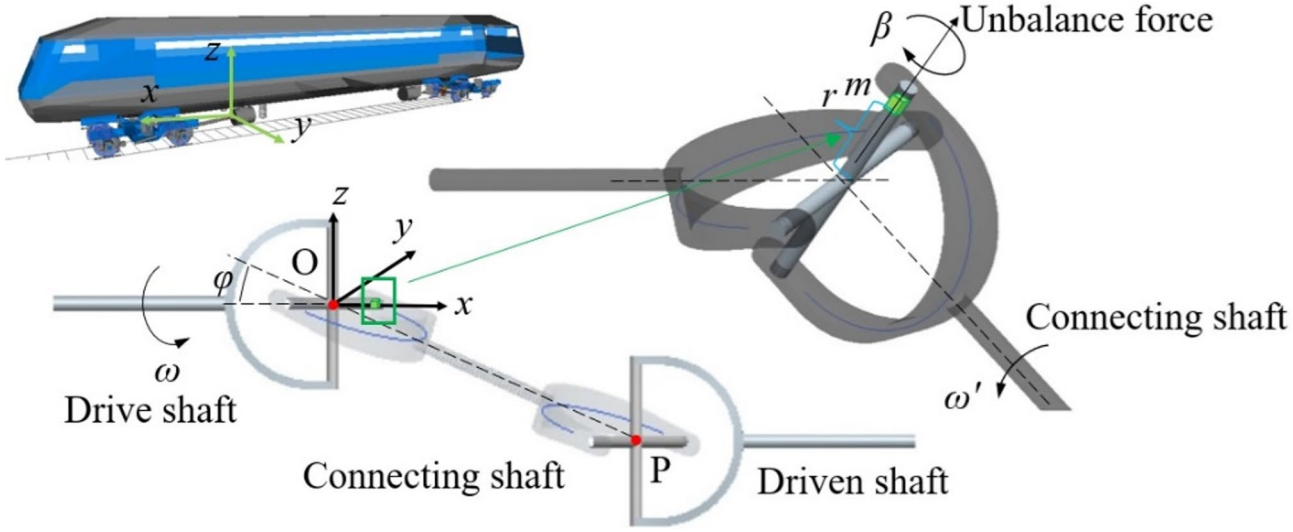

Fig. 2. Cardan joint transmission.

z_p=-0.045 m, and φ = 17.6 degrees. When the cardan shaft rotates at a frequency of 50 Hz with a static unbalance of 100 g·cm, the waveform and spectrum of the resulting unbalance force are shown in Fig. 3.

As shown in Fig. 3, the waveform of the unbalance force is close to a sinusoidal waveform, and the spectrum indicates that the amplitude of the spectral component corresponding to the rotating frequency (referred to as the main component) of the cardan shaft is much greater than that of the harmonic components. Therefore, the main component is prioritized for extraction to evaluate the static unbalance of the cardan shaft. The signal component corresponding to the main component is referred to as the unbalance signal. As the bandwidth of the unbalance signal is narrow, a narrow bandpass filter can be used to extract the unbalance signals from the measured acceleration signals. The Z-transform expression of a narrowband band-pass filter constructed using NZFF (hereinafter referred to as NZFF) is presented as follows.

$$H(z) = \frac{K\left(z^2 - 1\right)}{\left(z - \rho e^{j\Omega_c}\right)\left(z - \rho e^{-j\Omega_c}\right)} \tag{4}$$

$$K = \sqrt{\frac{\left[\rho^2 + \cos\left(2\Omega_c\right) - 2\rho\cos^2\left(\Omega_c\right)\right]^2 + \left[\sin\left(2\Omega_c\right)\left(1 - \rho\right)\right]^2}{2 - 2\cos\left(2\Omega_c\right)}}. \tag{5}$$

where ρ is a parameter of the filter and ρ is required to be less than 1. The term z equals to $e^{j\Omega}$, where the term Ω is the digital angular frequency. The term Ω_c denotes the target center frequency of the filter. To extract the unbalance signal, Ω is required to be $\Omega_c = \omega_c/f_s$, where f_s is the sampling frequency of the acceleration signal. The parameter K is a multiplier that ensures 0 dB gain of the filter at the target center frequency. The numerator of the constructed narrowband band-pass filter has two zero points, namely 0 and π, which indicates that the filter will eliminate the direct component from the signal. Compared with the case where no zero points are set in the numerator, defining these two zero points enhances the attenuation of frequency components other than the target frequency, thereby improving the filter's performance.

As ω_c varied continuously when the train speeds up or slows down, the target center frequency of NZFF is variable, and filtering of the signal is performed in discrete time segments. Therefore, bandwidth of the NZFF must cover variation of Ω_c within the subsequent time segments. Variation of Ω_c (denoted by $\Delta\Omega_c$) in the subsequent time segment is estimated through the obtained variation of Ω_c in the last time segment. Formula for estimating the $\Delta\Omega_c$ is given by Eq. (6).

$$\Delta\Omega_c = \Omega_c(t) - \Omega_c(t - \Delta T). \tag{6}$$

where the ΔT denotes the time length of the window for the estimation. Passband of the filter is defined as the band whose gain is greater than K_B (dB), which is the gain at the boundary of passband of the constructed filter. The boundary of the passband of the filter is set to $\Omega_B = \Omega_c + \Delta\Omega_c$, and a relation between frequency of the passband boundary and the gain of the filter at the boundary is given by Eq. (7).

$$\frac{\left[\rho^2 + \cos\left(2\Omega_B\right) - 2\rho\cos\left(\Omega_B\right)\cos\left(\Omega_c\right)\right]^2 + \left[\sin\left(2\Omega_B\right) - 2\rho\sin\left(\Omega_B\right)\cos\left(\Omega_c\right)\right]^2}{2 - 2\cos\left(2\Omega_B\right)} = \frac{K^2}{10^{0.1K_B}}. \tag{7}$$

Bisection algorithm or Newton-Raphson method can be applied to solve the parameter ρ from Eq. (7). The Z-transform of the filtering frame and the iterative filtering frame in time of the constructed filter are given by Eq. (8) and Eq. (9) respectively. The unbalance signal is extracted from the measured signal by implementing the filter.

$$\frac{Y(z)}{X(z)} = \frac{K\left(1 - z^{-2}\right)}{1 - 2\rho\cos\left(\Omega_c\right)z^{-1} + \rho^2 z^{-2}} \tag{8}$$

$$y(n) = 2\rho\cos\left(\Omega_c\right)y(n-1) - \rho^2 y(n-2) + Kx(n) - Kx(n-2). \tag{9}$$

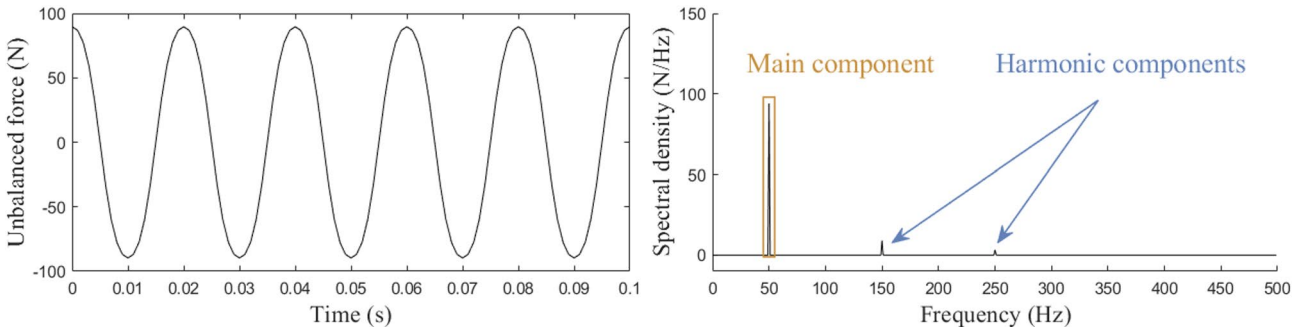

Fig. 3. Spectrum of the unbalance acceleration signal.

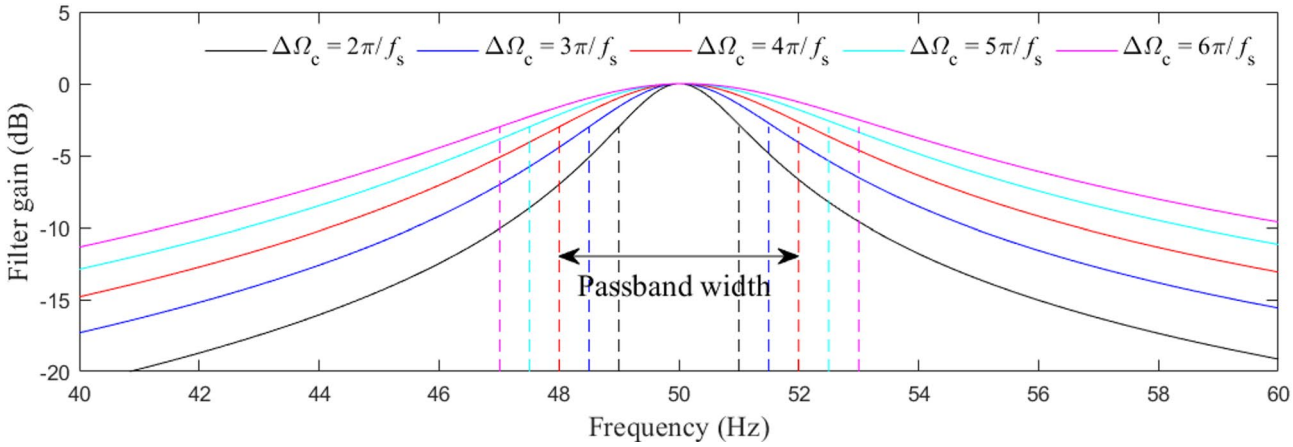

Fig. 4. Frequential responses of the constructed NZFF.

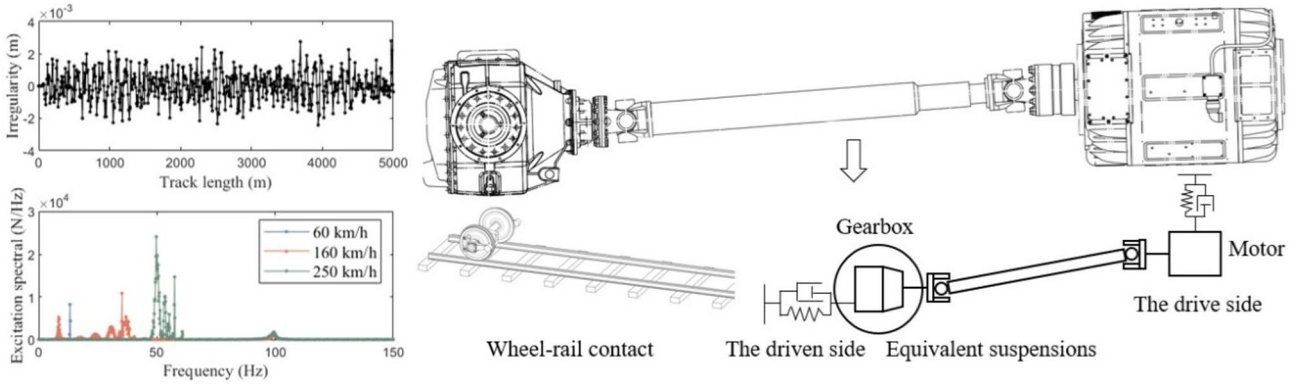

Fig. 5. Factors affecting the unbalance forces.

where $x(n)$ denotes the input signal, and $y(n)$ denotes the output signal. In practice, parameters of Eq. (9) are calculated at beginning of a new time segment, and the last two filter outputs in the last time segment are used as $y(n\text{-}2)$ and $y(n\text{-}1)$, respectively. Asking K_B=-3 dB, when $\Omega_c = 2\pi \times 50/f_s$, and $\Delta\Omega_c$ varies from $2\pi/f_s$ to $6\pi/f_s$, frequential responses of the constructed filter are presented in Fig. 4. As shown in the figure, the width of the passband of the filter increases as $\Delta\Omega_c$ rises, and the attenuation rate of the filter at different frequencies increases with the increase in $\Delta\Omega_c$.

Static unbalance evaluation

The amplitude of the unbalance force is proportional to the square of the circular frequency of the cardan shaft, resulting in variations in static unbalance evaluations performed at different train speeds. Moreover, as illustrated in Fig. 5, the spectra of kinematic excitations are distributed across a relatively broad frequency range, which may introduce random noise into the extracted signals and consequently lead to evaluation errors for the static unbalance. Additionally, the spectral density of the excitations increases with rising train speeds. This suggests that, although higher train speeds lead to larger amplitudes of unbalance forces, which is beneficial for the static unbalance evaluation, the noise associated with track irregularities degrades the evaluation conditions. Therefore, it is essential to suppress these noises.

As shown in Fig. 5, the transmission side of the cardan shaft closing to the gearbox is denoted by the driven side, and that closing to the motor is denoted by the drive side. Since integrating a sinusoidal signal superimposes a coefficient inversely proportional to the signal's circular frequency onto its amplitude and simultaneously attenuates high-frequency noise, a double-integration scheme in time based on the trapezoidal integration formula is constructed to achieve double integration of the NZFF's output signal. The Z-transform of the double-integration scheme expression is presented as follows:

$$\frac{S(z)}{Y(z)} = \frac{1}{4f_s^2} \cdot \frac{1 + 2z^{-1} + z^{-2}}{1 - 2z^{-1} + z^{-2}}. \tag{10}$$

where $Y(z)$ represents the Z-transform of the signal extracted by the NZFF, and $S(z)$ represents the Z-transform of the output signal of the double integration scheme. As shown in Eq. (2), the amplitude of the unbalance force

is directly proportional to the static unbalance. Therefore, the effective value of the integral of the extracted unbalance signal is adopted as an unbalance index to reflect the static unbalance of the cardan shaft.

$$I_{\mathrm{NZFF}}(n)=\sqrt{\frac{1}{N}\sum_{n=1}^{N}s^{2}(n)}. \tag{11}$$

where N is length of the acceleration signal in a time segment, and $s(n)$ denotes the output signal of the integral scheme. Given the relatively long length of the cardan shaft, the static unbalance of the cardan shaft is evaluated separately on the drive side and the driven side, with the evaluation positions located on the correction planes for the cardan shaft's two-plane dynamic balance. As torque is transmitted from the motor to the gearbox via the cardan shaft, the signal measured on the motor is defined as the drive-side signal, and the signal measured on the gearbox is defined as the driven-side signal. Although Eq. (2) indicate that the unbalance force of the cardan shaft is in direct proportion to the static unbalance, relation between the unbalance index and the static unbalance is not linear. This is because the suspension structures of the gearbox and the motor introduces a non-linear relationship between the vibrational responses at the measuring points and the unbalance forces, which means that the unbalance index will be amplified when the frequency of the unbalance signal is close to the natural frequency of the suspension structure.

As shown in Fig. 5, suspensions of the gearbox and the motor can be equivalent to a simple spring-damping structure. Since bandwidth of the extracted unbalance signal is narrow, the unbalance signal can be regarded as a single-frequency signal, the relation between the unbalance force and the unbalance index can be expressed by the transfer functions relating to the suspension structures.

$$\frac{I_{\mathrm{NZFF}}(n)}{F}=\left|\frac{1}{m\omega_{\mathrm{c}}^{2}-k-c\omega_{\mathrm{c}}\mathrm{j}}\right|. \tag{12}$$

where m, c, and k are the parameters of the equivalent suspension structure, which denote the mass, the damping, and the stiffness of the equivalent suspension, respectively, and j denotes the imaginary unit. An experiment has been conducted to determine the values of the above parameters, as demonstrated in the subsequent sections. The unbalance force can be determined through the unbalance index via Eq. (12) according to the circular frequency of the cardan shaft. Then the static unbalance of the cardan shaft is evaluated through Eq. (2).

$$U(n)=\left|m-\frac{k}{\omega_{\mathrm{c}}^{2}}-\frac{c}{\omega_{\mathrm{c}}}\mathrm{j}\right|\cdot I_{\mathrm{NZFF}}(n). \tag{13}$$

Due to the kinematic excitations generated by track irregularities, the static unbalance evaluated by Eq. (13) is unsteady, therefore, Kalman filter is utilized to stabilize the evaluated static unbalance. The processing progress adopting Kalman filter to stabilize the evaluated static unbalance is as follows.

$$\hat{U}_{n|n-1}(n)=\hat{U}_{n-1}(n-1) \tag{14}$$

$$P_{n|n-1}=P_{n-1|n-1}+Q \tag{15}$$

$$K_{k}=\frac{P_{n|n-1}}{P_{n|n-1}+R} \tag{16}$$

$$\hat{U}_{n}(n)=\hat{U}_{n|n-1}(n)+K_{n}\left(U(n)-\hat{U}_{n|n-1}(n)\right) \tag{17}$$

$$P_{n|n}=(1-K_{n})P_{n|n-1}. \tag{18}$$

where P denotes the covariance of error of the static unbalance predicted by Eq. (14), Q denotes the covariance of state variation noise of the static unbalance, R denotes the observation covariance of the static unbalance. The output $\widehat{U}_{n}(n)$ of the Kalman filter is adopted as the evaluation result of the static unbalance after stabilization.

Validation and comparison

Analyzation of signals acquired from line tests

The acceleration signals acquired from the line tests are utilized to illustrate the superiority of the proposed method in unbalance signal extraction and the static unbalance evaluation. The extracted unbalance signals and the unbalance indexes obtained by state-of-the-art techniques for addressing issues related to the unbalanced cardan shaft are used for the illustration, including EEMD, DDDR, and SVD. Two experimental cardan shafts are utilized in the line tests, and one of the cardan shafts is in an unbalanced condition, the other is normal. The conditions of the cardan shafts are defined by referencing the ISO 21940-11 standard, and the balance quality grade for the train's transmission cardan shaft is specified as level G40. Static unbalances of the cardan shafts used in the experiment are listed in Table 1. According to the maximum rotational speed and mass of the cardan shaft, the permissible residual unbalance of the cardan shaft under the level G40 is listed in Table 1 as well.

As listed in Table 1, under the level G40, the first cardan shaft is normal, and the second cardan shaft is in an unbalanced condition. Testing speeds of the experimental train varied from 100 km/h to 200 km/h, and

No.	Static unbalance (drive side)	Static unbalance (driven side)	Permissible residual unbalance (G40)	Condition
1	340 g cm	488 g cm	695 g cm	Normal
2	1130 g cm	842 g cm		Unbalanced

Table 1. Unbalances of the tested Cardan shafts.

No.	Speed (km/h)	Duration (s)
1	100	354
2	120	343
3	140	272
4	160	350
5	180	374
6	200	848

Table 2. Durations of the signal segments.

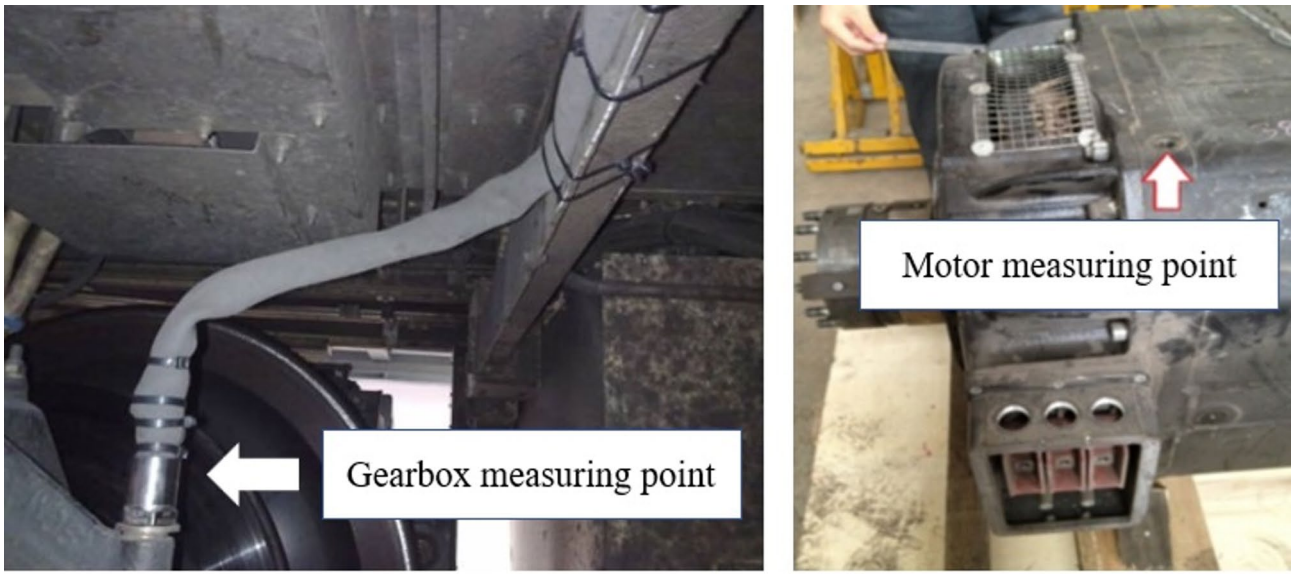

Fig. 6. The measuring points.

the acceleration signals are measured through sensors installed on the gearbox and the motor. The sampling frequency of the acceleration signal is set to 10^4 Hz. The sensors employed are single-axis piezoelectric accelerometers with threaded connections. They have a measurement range of ± 500 m/s² and a sensitivity of 10 mV/(m/s²). The durations of the signal segments at each speed level are presented in Table 2. The train speed, the measured signals, and the measuring points for measuring the acceleration signals are presented in Figs. 6 and 7, respectively.

Signals within two seconds under different speeds of the experimental train are used for the comparison. The decomposing level of DDDR is set to 5. Ratio of the standard deviation of the added noise and that of the input signal utilized by EEMD is set to 1. The maximum singular value of SVD is used for reconstructing the decomposed signal. Among all the reconstructed signals calculated by DDDR and EEMD, the one whose frequency is the closest to the circular frequency of the cardan shaft is chosen and regarded as the unbalance signal[21]. The unbalance signals extracted from the measured acceleration signals under the train speeds of 140 km/h and 160 km/h through different methods are presented in Figs. 8 and 9, respectively.

As presented in Fig. 8 (a), waveforms of the unbalance signals relating to the gearbox measuring point extracted by DDDR, and DDDR combined with SVD are more complicated, and it is hard to distinguish the unbalanced cardan shaft from the normal cardan shaft through amplitudes of the unbalance signals. The waveform of the unbalance signals relating to the gearbox measuring point extracted by the NZFF is close to a sine waveform with amplitude modulation, but the unbalanced cardan shaft can only be weakly distinguished from the normal cardan shaft. As presented in Fig. 8 (b), the extracted unbalance signals relating to the motor measuring point are sinusoidal and relatively steady except for that extracted by the EEMD. Differences between waveforms of the

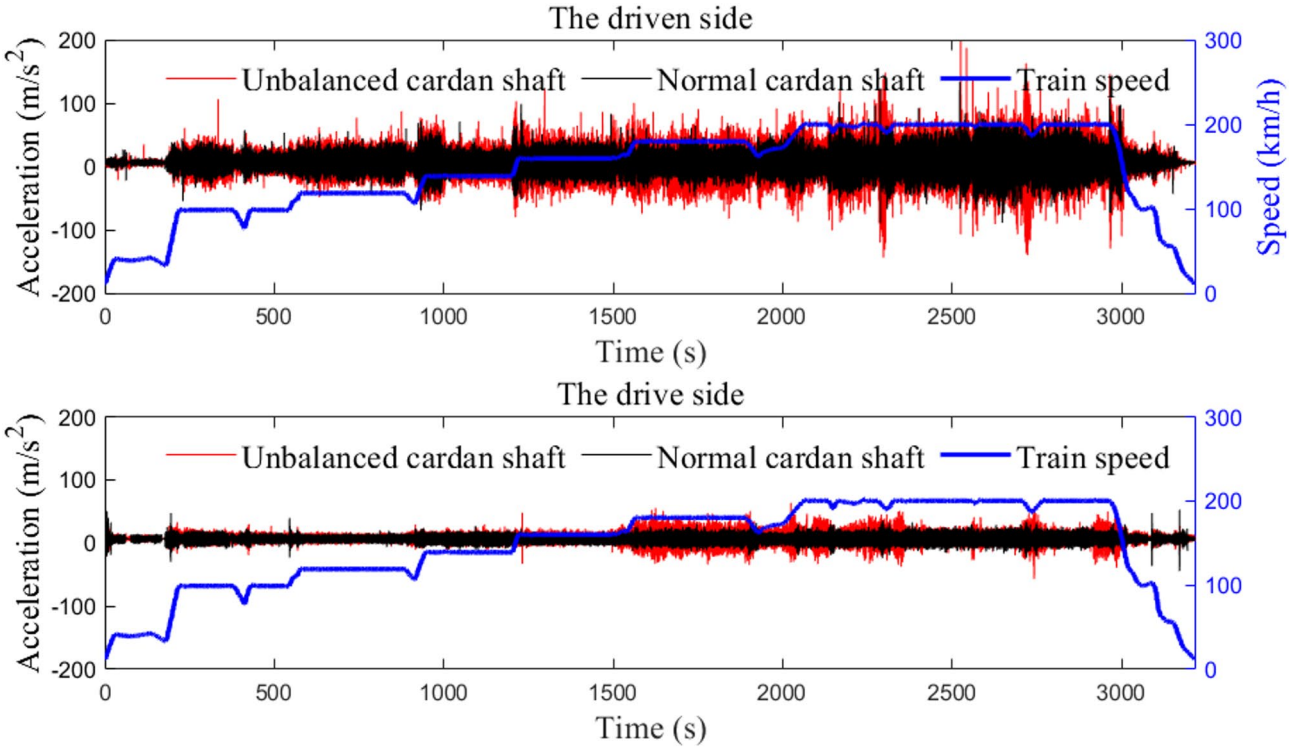

Fig. 7. Testing speed and the measuring points.

unbalance signals extracted by DDDR and DDDR combined with SVD are tiny, which indicated that function of the SVD is limited.

As presented in Fig. 9 (a), when the train speed reaches 160 km/h, the cardan shaft static unbalance becomes more easily distinguishable via the extracted signals relating to the signals measured on the gearbox, and the discrepancy in the amplitude of the signal extracted by the NZFF becomes more obvious. As shown in Fig. 9 (b), the discrepancies between the amplitudes of the extracted signals related to the signals measured on the motor for the unbalanced cardan shaft and those for the normal cardan shaft are evident. However, the signals extracted using the NZFF are much cleaner. The time costs for extracting the unbalance signals from the 2-second signals are presented in Table 3.

As shown in Table 3, the time costs for the DDDR method and the DDDR method combined with SVD are approximately 0.2 s, the time cost for the EEMD method exceeds 5 s, and the time cost for the NZFF method is less than 0.01 s. Therefore, the NZFF better satisfies the efficiency requirements for real-time evaluation of the static unbalance of the cardan shaft, while the EEMD method is not suitable for real-time condition monitoring of the cardan shaft due to its low efficiency.

To compare the differences in unbalance index values derived from the extracted signals at various train speeds, the average unbalance index values across different speed levels are calculated and are presented in Fig. 10.

As shown in Fig. 10 (a), the results for the signals measured on the gearbox indicate that the amplitudes of the indexes calculated by the NZFF for the unbalanced cardan shaft are significantly greater than those for the normal cardan shaft across different speed levels. In contrast, the indexes calculated using DDDR or DDDR combined with SVD fail to reflect the unbalanced condition of the cardan shaft at the speed level of 120 km/h, and the indexes calculated using EEMD fail to accurately reflect the unbalanced condition of the cardan shaft at both the 100 km/h and 120 km/h speed levels. As shown in Fig. 10 (b), except for the EEMD method, the indexes of the unbalanced cardan shaft calculated by other methods are all significantly greater than those of the normal cardan shaft. As a result, after extracting the unbalance signal using the NZZF method and performing double integration, the unbalance index of the extracted signal, calculated using Eq. (11), can better reflect the condition of the cardan shaft.

The structure parameters used in Eq. (13) to evaluate the static unbalance of the cardan shaft are identified using the average values of the unbalance indexes presented in Fig. 10. The matrix form of the relation between the parameters of the suspension structure and the unbalance indexes is given by Eq. (19), where the ω_{ck} denotes the k-th circular frequency of the cardan shaft, and $I_{NZFF}(\omega_{ck})$ denotes the average value of the unbalance index with respect to the k-th circular frequency ω_{ck}.

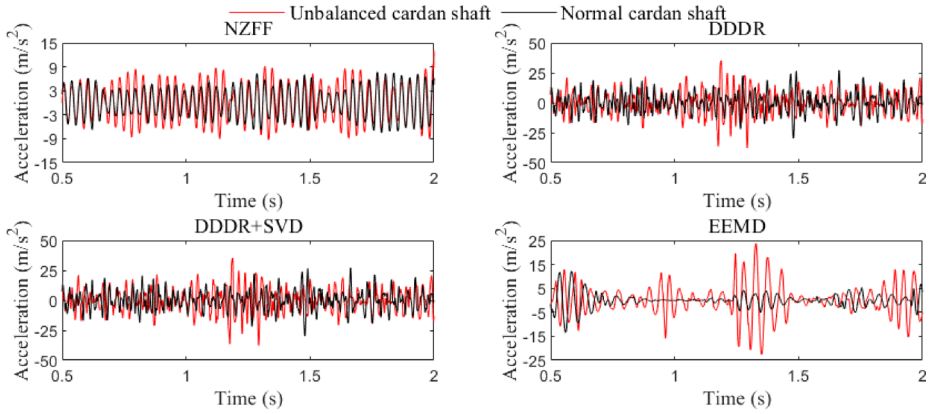

(a) Signals measured on the gearbox

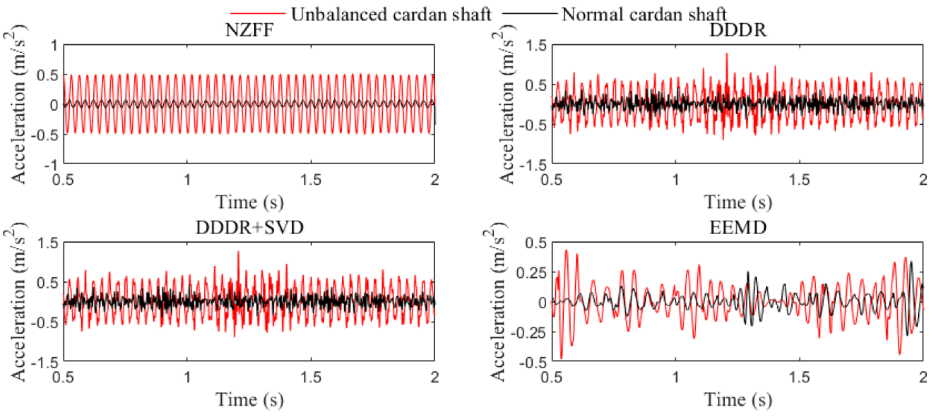

(b) Signals measured on the motor

Fig. 8. Comparison of results obtained at a train speed of 140 km/h.

$$\begin{bmatrix} 1 & \frac{1}{\omega_{c1}^2} & \frac{1}{\omega_{c1}^4} \\ \vdots & \vdots & \vdots \\ 1 & \frac{1}{\omega_{ck}^2} & \frac{1}{\omega_{ck}^4} \end{bmatrix} \begin{bmatrix} m^2 \\ c^2 - 2mk \\ k^2 \end{bmatrix} = \begin{bmatrix} \frac{m_r^2}{I_{NZFF}^2(\omega_{c1})} \\ \vdots \\ \frac{m_r^2}{I_{NZFF}^2(\omega_{ck})} \end{bmatrix}. \tag{19}$$

The unbalance index is obtained from the signals collected during all six speed levels. To fully utilize all unbalance indexes, the least squares method was employed to identify the parameters of the suspension structure. The equivalent form of the Eq. (19) can be expressed as $\boldsymbol{W}\cdot\boldsymbol{p}=\boldsymbol{\xi}$, and the least squares solution of the Eq. (19) is as follows.

$$\boldsymbol{p} = \left(\boldsymbol{W}^{\mathrm{T}}\boldsymbol{W}\right)^{-1}\boldsymbol{W}^{\mathrm{T}} \cdot \boldsymbol{\xi}. \tag{20}$$

The parameters of the equivalent suspension structures identified according to the unbalance indexes and the corresponding circular frequencies are listed in Table 4. Substituting the identified parameters into the Eq. (12), the unbalance indexes presented in Fig. 10, and the frequential responses calculated by the suspension structural parameters are presented in Fig. 11. For the convenience, the train speed corresponding to the circular frequencies of the cardan shaft are shown in the figure.

As shown in Fig. 11, the frequency responses calculated using the identified suspension structural parameters of the driven side match the indexes well when the train speed exceeds 160 km/h, while there are tiny discrepancies between the indexes and the responses at train speeds below 160 km/h. The frequency responses calculated using the identified suspension structural parameters of the drive side match the indexes well across all train speeds. The reason leading to the discrepancies is that the unbalance forces are weaker under

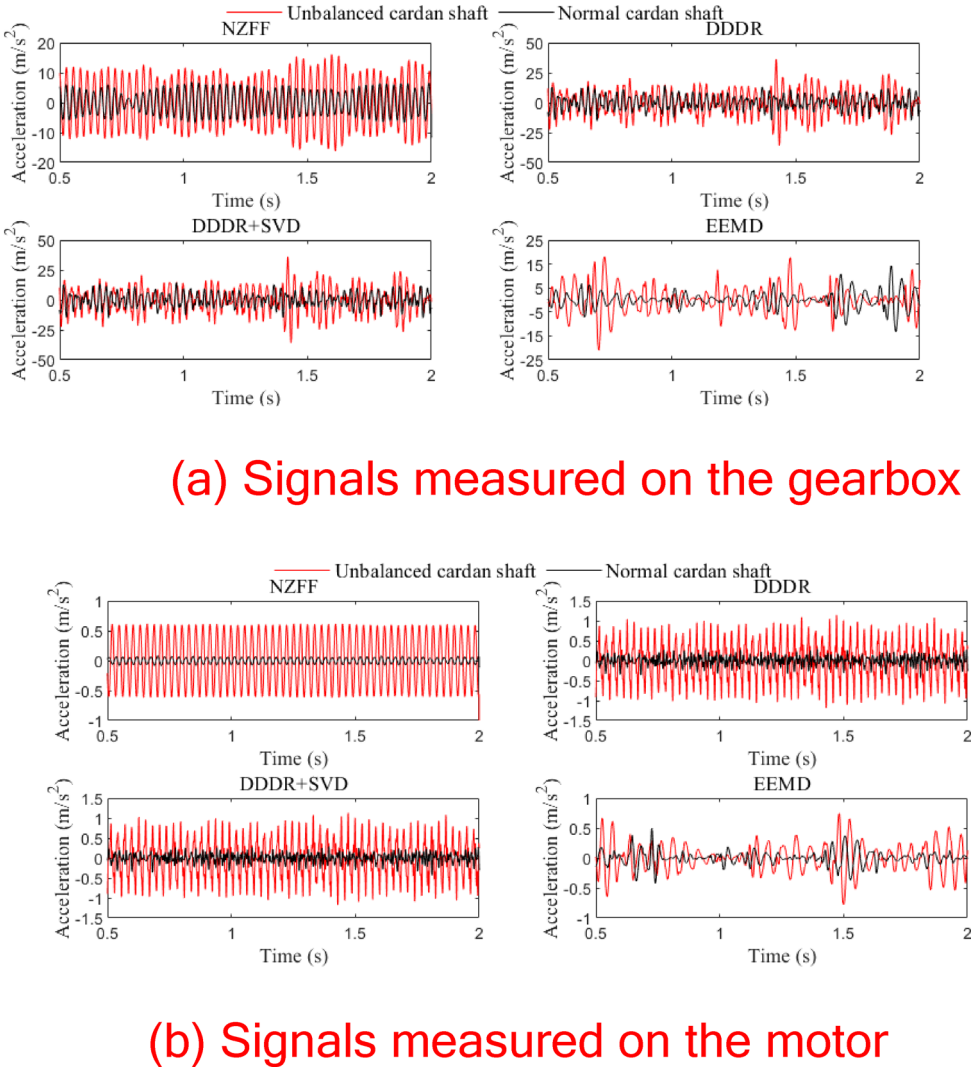

Fig. 9. Comparison of results obtained at a train speed of 160 km/h.

Method	Time cost (140 km/h)	Time cost (160 km/h)
NZFF	0.0013 s	0.0006 s
DDDR	0.1866 s	0.1836 s
DDDR + SVD	0.1882 s	0.1853 s
EEMD	5.8846 s	6.4442 s

Table 3. Time costs of extraction of the unbalance signal.

the relatively low train speeds, and the noises come from the track irregularities are easier to affect distributions of the unbalance indexes of the driven side under the train speeds, which diminished the index's capacity to accurately characterize the static unbalance.

Based on the values of the identified suspension structural parameters listed in Table 4, the evaluated static unbalances of the cardan shaft with respect to the driven side and the drive side calculated through Eq. (13) are presented in Fig. 12. As shown in the figure, the scatters of the unbalance indexes of the driven side distributed in a relatively wide range, while the scatters of the unbalance indexes of the drive side are obtained with relatively concentrated distributions. The evaluation results of the static unbalances closely match the preset values of the static unbalances for the experimental cardan shafts, demonstrating that after extracting the unbalance signals using the NZFF method, the double integration process combined with the unbalance calculation formula can accurately and effectively assess the static unbalance of the cardan shaft.

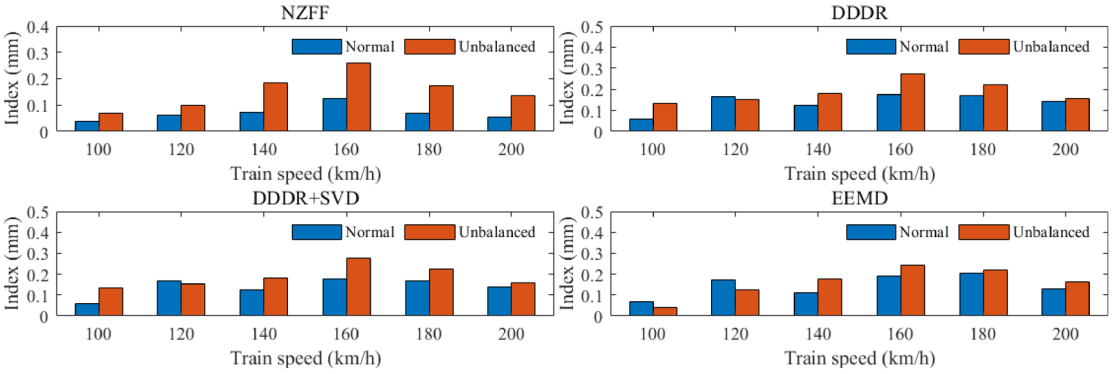

(a) Unbalance index obtained by the signals measured on the gearbox

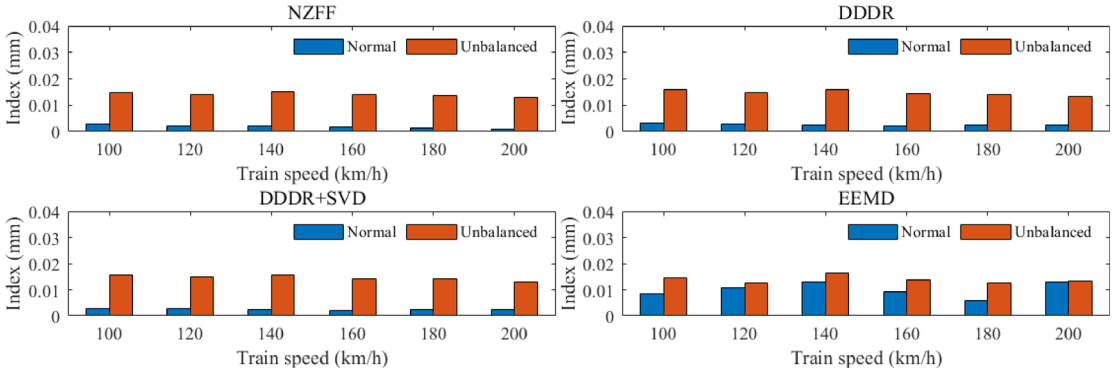

(b) Unbalance index obtained by the signals measured on the motor

Fig. 10. Unbalance indexes obtained by the different methods.

Gearbox			Motor		
m	**c**	**k**	**m**	**c**	**k**
140 kg	7×10^3 N m/s	6.5×10^6 N/m	950 kg	1×10^5 N m/s	1.4×10^7 N/m

Table 4. The identified transfer function parameters identified.

Analyzation of signals collected during train operation

Acceleration signals measured during train operation drew attention due to their excessive amplitudes, which triggered alarms from the devices monitoring condition of the cardan shaft. Subsequent maintenance confirmed that the corresponding cardan shaft exhibited a fault of excessive static unbalance. Waveforms of the acceleration signals are presented in Fig. 13(a), and the static unbalances measured via dynamic balance measuring instrument are shown in Fig. 13(b). As presented in Fig. 13, the maximum speed of the train with respect to the measured signals is about 200 km/h, and the measured static unbalances are 1718 g cm of the drive side, and 2218 g cm of the driven side, respectively. According to the general dispersions of the unbalance indexes obtained by the NZFF, the observation covariance R of the Kalman filter with respected to the driven side is set to 40 when

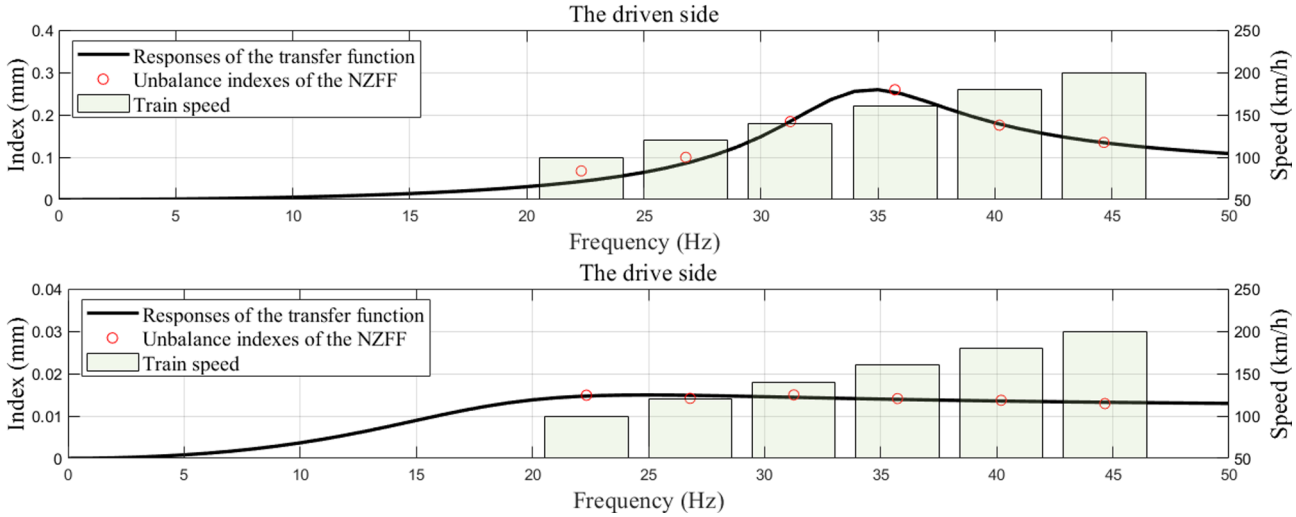

Fig. 11. Unbalance indexes and frequency responses of the suspension structures.

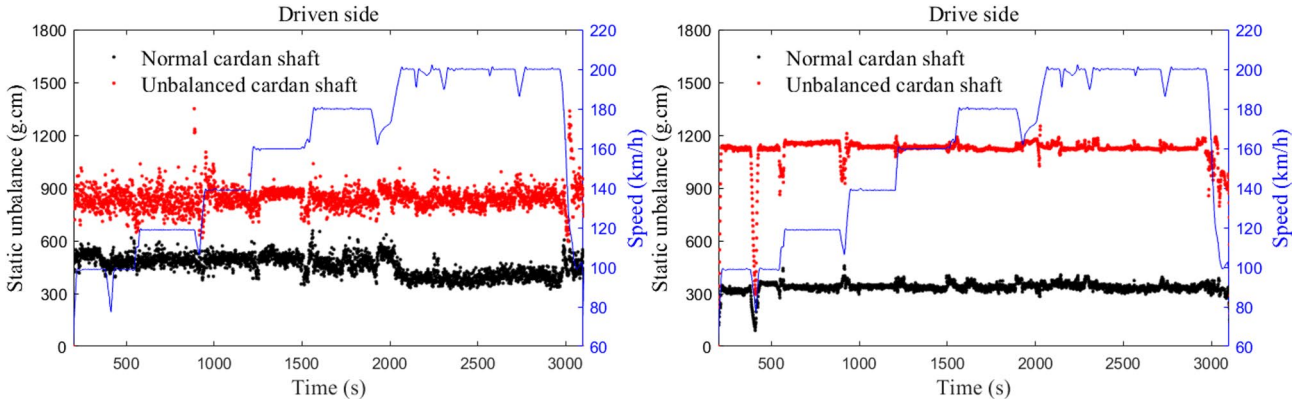

Fig. 12. Scatter diagram of the unbalance indexes obtained by NZFF.

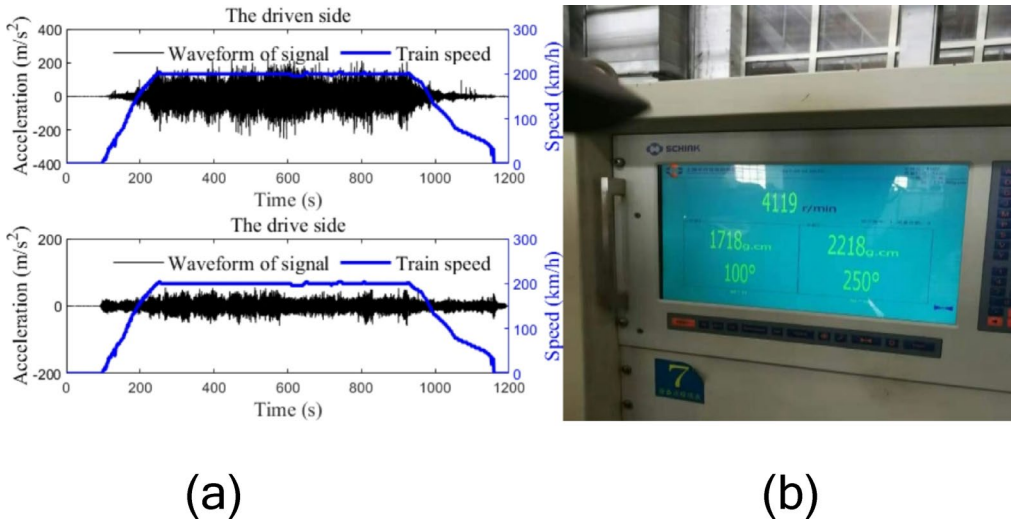

Fig. 13. The measured signal and the measured static unbalance of the cardan shaft. (**a**) Waveforms of the measured signal. (**b**) The measured static unbalances.

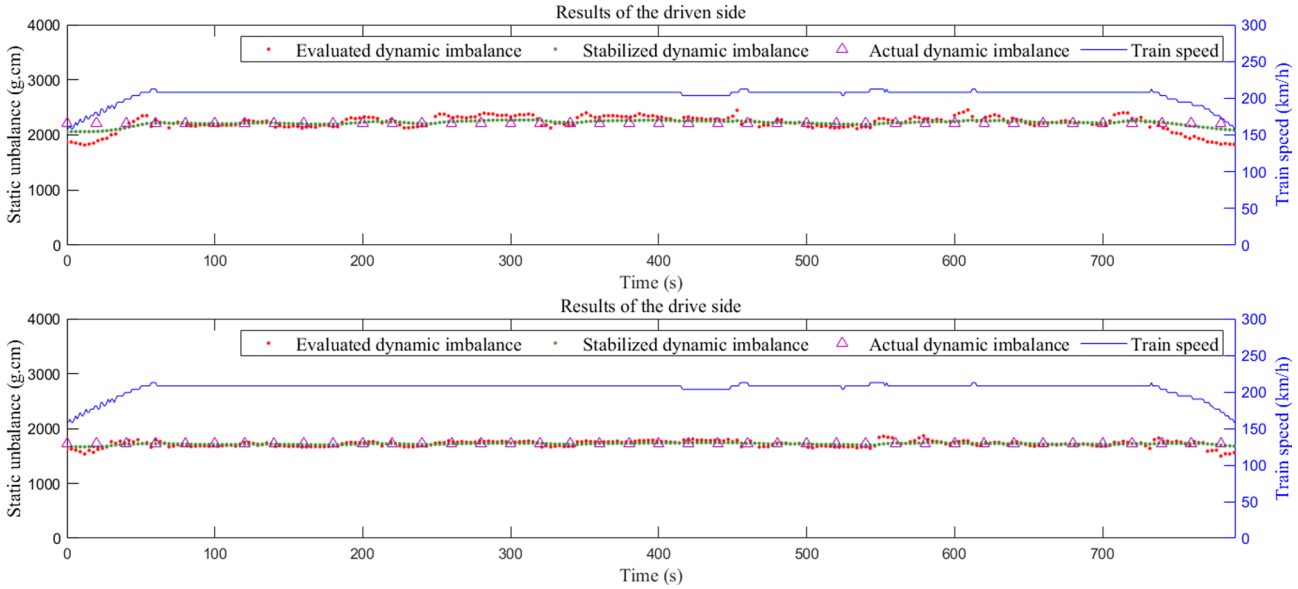

Fig. 14. The evaluated static unbalances.

the train speed is below 160 km/h, and the R is set to 23 when the train speed exceeds 160 km/h. The R with respected to the drive side is set to 0.4. As variation of static unbalance of the cardan shaft during operation is tiny, Q is set to 0.1. The initial covariance of the prediction error is set to $P_0 = 1$. The evaluated static unbalances of the cardan shaft with respect to the train speeds exceeding 160 km/h are shown in Fig. 14.

As shown in Fig. 14, the evaluated static unbalances are largely consistent with the actual static unbalances of the cardan shaft. The maximum differences between the evaluated and actual static unbalances at the driven side and drive side are 399 g·cm and 223 g·cm, respectively. The maximum differences between the stabilized static unbalances and the actual static unbalances at the driven side and drive side are 161 g·cm and 54 g·cm, respectively. Consequently, the Kalman filter demonstrates a pronounced stabilizing effect on the evaluated static unbalances.

Although the static unbalance of the cardan shaft is evaluated accurately by adopting the NZFF when the train speeds exceeded 160 km/h, the NZFF failed to evaluate the static unbalance under the relatively low train speeds. Therefore, developing methods mitigating noises of the unbalance signals extracted under relatively low speeds of the train is the research objective in the future studies.

Conclusion

As the static unbalance of the cardan shaft used in the high-speed train does harm to driving safety and stability, a method is proposed in this study to real-time evaluate static unbalance of the cardan shaft. The NZFF method is employed to extract the unbalance signal from the measured signal. Subsequently, double integration is applied to the extracted signal to eliminate the influence of circular frequency on the signal amplitude and reduce signal noise. Efficient value of the extracted signal is used as an index to evaluate the static unbalance of the cardan shaft. Based on the identified parameters of the suspension structures, the static unbalance is evaluated according to the unbalance index and the circular frequency. The Kalman filter is used to enhance stability of the evaluated results. The key conclusions of this study are as follows:

1. Compared with the other existing methods for addressing issues related to the unbalanced cardan shaft used in the high-speed train, the unbalance signals extracted by the NZFF are obtained superior performance in condition distinguishing of the cardan shaft.
2. The extraction of the unbalance signal implemented by the NZFF is relatively more efficient, so that the NZFF is more suitable for the real-time evaluation of static unbalance of the cardan shaft.
3. Due to the influence of the suspension structure in the cardan shaft transmission system, the value of the unbalance index is affected. By modeling the suspension structure as a spring-damper system and analyzing its transfer function characteristics, the unbalanced force can be inferred, enabling the evaluation of the static unbalance.
4. More noise is mixed in with the extracted unbalance signals of the driven side, leading to dispersion in the evaluated static unbalances of the driven side, while the evaluated static unbalances of the drive side are more concentrated.

Data availability

The datasets used during the current study available from the corresponding author on reasonable request. All data generated or analyzed during this study are included in this published article and its supplementary information files.

Received: 23 January 2025; Accepted: 26 May 2025
Published online: 02 June 2025

References

1. Hu, Y., Zhang, B. & Tan, A. C. Acceleration signal with DTCWPT and novel optimize SNR index for diagnosis of misaligned Cardan shaft in high-speed train. *Mech. Syst. Signal. Process.* **140**, 106723. https://doi.org/10.1016/j.ymssp.2020.106723 (2020).
2. Hu, Y., Lin, J. & Tan, A. C. Failure analysis of gearbox in CRH high-speed train. *Eng. Fail. Anal.* **105**, 110–126. https://doi.org/10.1016/j.engfailanal.2019.06.099 (2019).
3. Hu, Y., Chit Tan, A., Liang, C. & Li, Y. Failure analysis of fractured motor bolts in high-speed train due to Cardan shaft misalignment. *Eng. Fail. Anal.* **122**, 105246. https://doi.org/10.1016/j.engfailanal.2021.105246 (2021).
4. Yongxu, H., Chit, A., Cai, Y. & Fengming, L. Effect analysis of Cardan shaft misalignment on dynamic performance of high-speed vehicle. *Eng. Fail. Anal.* **150**, 107301. https://doi.org/10.1016/j.engfailanal.2023.107301 (2023).
5. Chen, C. K. & Freudenstein, F. Dynamic analysis of a universal joint with manufacturing tolerances. *J. Mech. Transm Autom. Des.* **108** https://doi.org/10.1115/1.3258764 (1986).
6. Patel, T. H. & Darpe, A. K. Vibration response of misaligned rotors. *J. Sound Vib.* **325**, 609–628. https://doi.org/10.1016/j.jsv.2009.03.024 (2009).
7. Patel, T. H. & Darpe, A. K. Experimental investigations on vibration response of misaligned rotors. *Mech. Syst. Signal. Process.* **23**, 2236–2252. https://doi.org/10.1016/j.ymssp.2009.04.004 (2009).
8. Patel, T. H. & Darpe, A. K. Vibration response of a cracked rotor in presence of rotor-stator Rub. *J. Sound Vib.* **317**, 841–865. https://doi.org/10.1016/j.jsv.2008.03.032 (2008).
9. Verma, A. K., Sarangi, S. & Kolekar, M. H. Experimental investigation of misalignment effects on rotor shaft vibration and on stator current signature. *J. Fail. Anal. Prev.* **14**, 125–138. https://doi.org/10.1007/s11668-014-9785-7 (2014).
10. Lu, J. W., Wang, G. C., Chen, H., Vakakis, A. F. & Bergman, L. A. Dynamic analysis of cross shaft type universal joint with clearance. *J. Mech. Sci. Technol.* **27**, 3201–3205. https://doi.org/10.1007/s12206-013-0842-z (2013).
11. Omar, M. H., Rahim, M. A. & Rejab, M. N. A. M. Numerical study on effect of phase angle on torsional and lateral vibrations in power transmission system employing Cardan shaft. *J. Teknol.* **85**, 113–122. https://doi.org/10.11113/jurnalteknologi.v85.19645 (2023).
12. Tchomeni, B. X. & Alugongo, A. Theoretical and experimental analysis of an unbalanced and cracked Cardan shaft in the vicinity of the critical speed. *Math. Model. Eng.* **6**, 34–49. https://doi.org/10.21595/mme.2019.21240 (2020).
13. Xia, Y., Pang, J., Yang, L., Zhao, Q. & Yang, X. Nonlinear numerical and experimental study on the second-order torsional and lateral vibration of driveline system connected by Cardan joint. *JVC/Journal Vib. Control.* **26**, 540–551. https://doi.org/10.1177/1077546319889846 (2020).
14. SoltanRezaee, M., Ghazavi, M. R., Najafi, A. & Rahmanian, S. Stability of a multi-body driveshaft system excited through U-joints. *Meccanica* **53**, 1167–1183. https://doi.org/10.1007/s11012-017-0784-0 (2018).
15. SoltanRezaee, M., Ghazavi, M. R. & Najafi, A. Parametric resonances for torsional vibration of excited rotating machineries with nonconstant velocity joints. *JVC/Journal Vib. Control.* **24**, 3262–3277. https://doi.org/10.1177/1077546317703542 (2018).
16. Bharti, S. K. & Samantaray, A. K. Resonant capture and Sommerfeld effect due to torsional vibrations in a double Cardan joint driveline. *Commun. Nonlinear Sci. Numer. Simul.* **97**, 105728. https://doi.org/10.1016/j.cnsns.2021.105728 (2021).
17. Yao, W. & Desmidt, H. Nonlinear coupled torsion/lateral vibration and Sommerfeld behavior in a double U-Joint driveshaft. *J. Vib. Acoust.* **143**, 1–15. https://doi.org/10.1115/1.4048558 (2021).
18. Ding, J., Lin, J. & Yu, S. Dynamic unbalance detection of Cardan shaft in high-speed train applying double decomposition and double reconstruction method. *Meas. J. Int. Meas. Confed.* **73**, 111–120. https://doi.org/10.1016/j.measurement.2015.05.016 (2015).
19. Zheng, Z., Lin, J., Hu, Y., Zhou, Q. & Yi, C. Dynamic unbalance identification and quantitative diagnosis of Cardan shaft in high-speed train based on improved TQWT-RBFNN-NSGA-II method. *Eng. Fail. Anal.* **136**, 106226. https://doi.org/10.1016/j.engfailanal.2022.106226 (2022).
20. Ding, J. M., Lin, J. H., He, L. & Zhao, J. Dynamic unbalance detection of Cardan shaft in high-speed train based on EMD-SVD-NHT. *J. Cent. South. Univ.* **22**, 2149–2157. https://doi.org/10.1007/s11771-015-2739-8 (2015).
21. Yi, C., Lin, J., Ruan, T. & Li, Y. Real time Cardan shaft state Estimation of High-Speed train based on ensemble empirical mode decomposition. *Shock Vib.* **2015** https://doi.org/10.1155/2015/912483 (2015).
22. Li, Y., Zuo, M. J., Chen, Z. & Lin, J. Railway bearing and Cardan shaft fault diagnosis via an improved morphological filter. *Struct. Heal Monit.* **19**, 1471–1486. https://doi.org/10.1177/1475921719886067 (2020).
23. Wu, W., Xiao, Y., Lin, J., Ma, L. & Khorasani, K. An efficient filter bank structure for adaptive Notch filtering and applications, **29** 3226–3241. (2021).
24. Blaut, J. & Brenkacz, Ł. Application of the dispersion entropy with sliding window for the analysis of mechanical systems. *Diagnostyka* **25**, 1–12. https://doi.org/10.29354/diag/195473 (2024).
25. Guo, J. et al. Transient impulses enhancement based on adaptive multi-scale improved differential filter and its application in rotating machines fault diagnosis. *ISA Trans.* **120**, 271–292. https://doi.org/10.1016/j.isatra.2021.03.005 (2022).
26. Wang, S., Chen, B., Cheng, Y. & Jiang, X. Investigation on morphological filtering via enhanced adaptive time-varying structural element for bearing fault diagnosis. *Meas. J. Int. Meas. Confed.* **244**, 116466. https://doi.org/10.1016/j.measurement.2024.116466 (2025).
27. Prasad, R., Yilmaz, G., Chetelat, O., Magimai.-Doss, M. & Of, D. 1 and S2 locations in phonocardiogram signals using zero frequency filter, in: ICASSP 2020–2020 IEEE int. Conf. Acoust. *Speech Signal. Process.* 1254–1258. https://doi.org/10.1109/ICASSP40776.2020.9053155 (2020).
28. Shukla, S., Singh, S. K. & Mitra, D. An efficient heart sound segmentation approach using kurtosis and zero frequency filter features. *Biomed. Signal. Process. Control.* **57**, 101762. https://doi.org/10.1016/j.bspc.2019.101762 (2020).
29. Chauhan, P. & Kumar Singh, S. A multi-frequency approach for the fault identification of bearings and gears based on frequency shifting and narrowband filtering. *Nondestruct Test. Eval.* **00**, 1–34. https://doi.org/10.1080/10589759.2024.2433034 (2024).
30. Murty, K. S. R. & Yegnanarayana, B. Epoch extraction from speech signals. *IEEE Trans. Audio Speech Lang. Process.* **16**, 1602–1613. https://doi.org/10.1109/TASL.2008.2004526 (2008).
31. Kumar, K., Shukla, S. & Singh, S. K. Early detection of bearing faults using minimum entropy Deconvolution adjusted and zero frequency filter. *JVC/Journal Vib. Control.* **28**, 1011–1024. https://doi.org/10.1177/1077546320986368 (2022).
32. Sachan, S., Shukla, S. & Singh, S. K. Two level de-noising algorithm for early detection of bearing fault using wavelet transform and zero frequency filter. *Tribol Int.* **143**, 106088. https://doi.org/10.1016/j.triboint.2019.106088 (2020).

Acknowledgements

The work is supported by the Natural Science Foundation of Sichuan Province (Grants No. 2022NSFSC1910, and No. 2023NSFSC0864)).

Author contributions

Hu Yongxu wrote and reviewed the main manuscript text. Luo Kang prepared Figs. 1 and 5. Yang Yaru programed the algorithm. Luo Yan collected the data for this study.

Declarations

Competing interests

The authors declare no competing interests.

Additional information

Supplementary Information The online version contains supplementary material available at https://doi.org/10.1038/s41598-025-04221-y.

Correspondence and requests for materials should be addressed to H.Y.

Reprints and permissions information is available at www.nature.com/reprints.

Publisher's note Springer Nature remains neutral with regard to jurisdictional claims in published maps and institutional affiliations.

Open Access This article is licensed under a Creative Commons Attribution-NonCommercial-NoDerivatives 4.0 International License, which permits any non-commercial use, sharing, distribution and reproduction in any medium or format, as long as you give appropriate credit to the original author(s) and the source, provide a link to the Creative Commons licence, and indicate if you modified the licensed material. You do not have permission under this licence to share adapted material derived from this article or parts of it. The images or other third party material in this article are included in the article's Creative Commons licence, unless indicated otherwise in a credit line to the material. If material is not included in the article's Creative Commons licence and your intended use is not permitted by statutory regulation or exceeds the permitted use, you will need to obtain permission directly from the copyright holder. To view a copy of this licence, visit http://creativecommons.org/licenses/by-nc-nd/4.0/.

© The Author(s) 2025